

Drive Fast, Learn Faster: On-Board RL for High Performance Autonomous Racing

Benedict Hildisch, Edoardo Ghignone, Nicolas Baumann, Cheng Hu, Andrea Carron, Michele Magno

Keywords: Autonomous Racing, Physical Robot Learning,

Summary

Autonomous racing presents unique challenges due to its non-linear dynamics, the high speed involved, and the critical need for real-time decision-making under dynamic and unpredictable conditions. Most traditional [Reinforcement Learning \(RL\)](#) approaches rely on extensive simulation-based pre-training, which faces crucial challenges in transfer effectively to real-world environments. This paper introduces a robust on-board [RL](#) framework for autonomous racing, designed to eliminate the dependency on simulation-based pre-training enabling direct real-world adaptation. The proposed system introduces a refined [Soft Actor-Critic \(SAC\)](#) algorithm, leveraging a residual [RL](#) structure to enhance classical controllers in real-time by integrating multi-step [Temporal-Difference \(TD\)](#) learning, an asynchronous training pipeline, and [Heuristic Delayed Reward Adjustment \(HDRA\)](#) to improve sample efficiency and training stability. The framework is validated through extensive experiments on the FITENTH racing platform, where the residual [RL](#) controller consistently outperforms the baseline controllers and achieves up to an 11.5% reduction in lap times compared to the [State-of-the-Art \(SotA\)](#) with only 20 min of training. Additionally, an [End-to-End \(E2E\)](#) [RL](#) controller trained without a baseline controller surpasses the previous best results with sustained on-track learning.

Contribution(s)

1. This paper presents an efficient [RL](#) architecture, based on the residual policy structure, that enables uninterrupted on-board learning at an unprecedented level of performance. The architecture is compared to an [E2E](#) structure, showing how the residual policy greatly increases efficiency by simplifying the control task.
Context: The work by [Stachowicz et al. \(2023\)](#) presented a high-speed driving solution with on-vehicle data only but failed to compare with [SotA](#) traditional methods for racing, exhibiting a performance gap. We show how a residual structure, previously used by [Trumpp et al. \(2023\)](#) in simulation, can be used to efficiently train in reality only and overtake classical [SotA](#) performance.
2. This paper compares different baseline controllers with the residual [RL](#) policy, showing how the proposed architecture is easily adaptable and improves on all the methods. The fastest agent in the comparison eventually turns out to be the fastest FITENTH algorithm when compared to previous best results.
Context: The work by [Trumpp et al. \(2023\)](#) only used [Pure Pursuit \(PP\)](#) as a baseline controller, while we show that the residual architecture can also adapt to different ones.
3. This paper provides an ablation study in the FITENTH simulation environment of the different [RL](#) architectural choices, showing how the different parts affect efficiency and training consistency.
Context: Some of the architectural choices were motivated by previous ablation studies (multi-step [TD](#) by [Barth-Maron et al. \(2018\)](#), asynchronous training by [Yuan & Mahmood \(2022\)](#)). Here the full combination is tested in the [Autonomous Racing \(AR\)](#) environment. Furthermore, the introduction of the novel [HDRA](#) is analyzed.
4. This paper provides a generalization study showing how the residual policy behaves with a different type of track and tires in a zero-shot and few-shot setup.
Context: None

Drive Fast, Learn Faster: On-Board RL for High Performance Autonomous Racing

Benedict Hildisch^{1,†}, Edoardo Ghignone^{1,†}, Nicolas Baumann¹, Cheng Hu²,
Andrea Carron³, Michele Magno¹

edoardo.ghignone@pbl.ee.ethz.ch

¹Center for Project-Based Learning, D-ITET, ETH Zurich

²Department of Control Science and Engineering, Zhejiang University

³Institute for Dynamic Systems and Control, D-MAVT, ETH Zurich

[†]Equal Contribution

Abstract

Autonomous racing presents unique challenges due to its non-linear dynamics, the high speed involved, and the critical need for real-time decision-making under dynamic and unpredictable conditions. Most traditional [Reinforcement Learning \(RL\)](#) approaches rely on extensive simulation-based pre-training, which faces crucial challenges in transfer effectively to real-world environments. This paper introduces a robust on-board [RL](#) framework for autonomous racing, designed to eliminate the dependency on simulation-based pre-training enabling direct real-world adaptation. The proposed system introduces a refined [Soft Actor-Critic \(SAC\)](#) algorithm, leveraging a residual [RL](#) structure to enhance classical controllers in real-time by integrating multi-step [Temporal-Difference \(TD\)](#) learning, an asynchronous training pipeline, and [Heuristic Delayed Reward Adjustment \(HDRA\)](#) to improve sample efficiency and training stability. The framework is validated through extensive experiments on the F1TENTH racing platform, where the residual [RL](#) controller consistently outperforms the baseline controllers and achieves up to an 11.5% reduction in lap times compared to the [State-of-the-Art \(SotA\)](#) with only 20 min of training. Additionally, an [End-to-End \(E2E\)](#) [RL](#) controller trained without a baseline controller surpasses the previous best results with sustained on-track learning. These findings position the framework as a robust solution for high-performance autonomous racing and a promising direction for other real-time, dynamic autonomous systems.

1 Introduction

[Reinforcement Learning \(RL\)](#) has become ubiquitous in robotics, particularly on quadrupedal robots, [RL](#) is now almost indispensable for locomotion, as it implicitly learns efficient heuristics for complex movements [Hoeller et al. \(2024\)](#). Similarly, in autonomous drone racing, [RL](#) has exhibited superhuman control capabilities, outperforming traditional approaches and human champions [Kaufmann et al. \(2023\)](#). These successes highlight the necessity of [RL](#) in robotics, particularly for pushing robotic systems to their performance limits.

Despite its success in various robotic domains, [RL](#) has not yet achieved widespread adoption in [Autonomous Racing \(AR\)](#). This is particularly notable, given that [AR](#) also involves agile control of non-linear systems posing significant challenges for robotic platforms ([Betz et al., 2023](#)). Moreover, the few solutions found on [AR](#) are showing impressive results only in simulation ([Fuchs et al., 2021](#);

Vasco et al., 2024), while evaluations on physical race cars remain limited. One possible explanation is due to the fact that when deployed on real vehicles, RL-based controllers are consistently slower than State-of-the-Art (SotA) classical AR controllers (Brunnbauer et al., 2022; Ghignone et al., 2025). This suggests that the Simulation-to-Reality (sim-to-real) gap in AR is particularly challenging to bridge.

One approach to mitigating this gap involves developing high-fidelity simulators that accurately model vehicle dynamics, adapting them to every possible physical environment. While this approach has been effective, especially in tandem with data-driven techniques that improve simulation accuracy (Kaufmann et al., 2023), it remains limited by inevitable mismatches between simulated and real-world physics and requires accurate system identification of the physical system and calibration of the simulator (Song et al., 2023). Instead, we take a different approach, bypassing these limitations entirely by training directly on the physical car and allowing the agent to learn and adapt to real-world dynamics from the start.

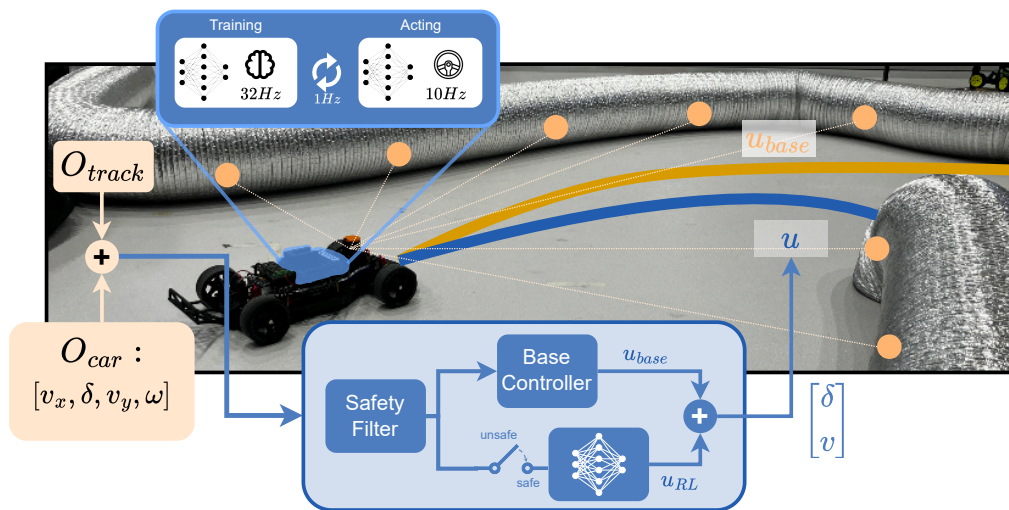


Figure 1: Overview of the proposed RL architecture, which processes observations O_{car} , providing proprioceptive information such as position and velocity (v_x ; v_y), and O_{track} , describing track boundaries and a given reference trajectory to generate a residual control command u_{RL} . Such a command is additively combined with the output of a conventional controller u_{base} . Since the agent starts untrained and may encounter unsafe states, a safety filter is employed to guide the robot back to a safe state. Training happens entirely on-board in an asynchronous fashion: the Acting node provides residual control commands at 10 Hz, while the training node updates the control policy at 32 Hz. The policy of the acting node is updated with the policy of the training node every second.

This work proposes an onboard RL-based high-performance AR controller that significantly and consistently outperforms SotA classical controllers in terms of lap time. This work eliminates the sim-to-real gap by training the RL agent (Wu et al., 2023; Stachowicz et al., 2023) directly on the physical robot, namely a 1:10 scaled FITENTH race car (O’Kelly et al., 2020), and validates the approach across multiple track layouts and friction conditions. With accurate real-world measurements, this paper demonstrates that an RL agent can out-perform a model-based SotA racing controller in real-world AR. The presented method achieves up to a 11.5% improvement in lap time, and enables the physical robot to operate without speed constraints and over 6.5 m s^{-1} . Moreover, one important finding out of this approach is that direct on-robot training introduces a new challenge: unlike simulation, where massive parallelization can be leveraged to accelerate learning (Rudin et al., 2021), real-world training remains inherently limited by the time needed for data collection. To address this problem, a residual RL structure is employed (Johannink et al., 2019), enabling a fully untrained agent to learn to exceed the performance of the SotA controller within 20 min. This paper further shows that such architecture significantly accelerates the training process, as an End-

to-End (E2E) model (not residual), achieves similar but slower lap times in three times the amount of training.

The proposed training framework is based on the **Soft Actor-Critic (SAC)** algorithm and incorporates several modifications to facilitate on-board learning. Multi-step **Temporal-Difference (TD)** updates are utilized to manage delayed rewards (Sutton & Barto, 2018), while **Heuristic Delayed Reward Adjustment (HDRA)**, inspired by **Hindsight Experience Replay (HER)**, is employed to emphasize undesirable behaviors. Additionally, an asynchronous training pipeline is implemented, decoupling data collection from policy optimization, following the approach of Yuan & Mahmood (2022). Finally, a safety filter allows for uninterrupted data collection, by gating potentially unsafe inputs and rerouting the vehicle to a reference safe trajectory. An overview of the proposed architecture is available in Figure 1.

2 Related Work

RL has seen growing applications in **AR** due to its potential to handle high-speed decision-making and complex, non-linear vehicle dynamics (Fuchs et al., 2021; Vasco et al., 2024). While this section focuses on previous work that directly informs our approach, Appendix A gives a broader overview of the advancements in autonomous driving and its subfield **AR**.

The **Sim-to-real gap** has been a persistent issue in applying **RL** to physical **AR** systems (Zhao et al., 2020). This gap stems from the inability of simulators to accurately replicate real-world dynamics, sensor noise, latencies, and environmental uncertainties. Methods such as system identification (Sontakke et al., 2023) and domain randomization (Tobin et al., 2017; Peng et al., 2018) have been widely adopted to address this problem. Chisari et al. (2021) proposed an **RL** framework for miniature race cars that leveraged model randomization, policy regularization, and online fine-tuning of the learned policy to diminish the **sim-to-real** gap, achieving near **Model Predictive Control (MPC)**-level performance. Despite these advances, **sim-to-real** methods often require extensive pre-training in simulation and substantial fine-tuning on physical systems, which can be resource-intensive and time-consuming and do not reach the performance of classical **SotA** controllers. Our proposed architecture bypasses these problems entirely by learning directly on-board.

Residual RL (Johannink et al., 2019) proposes a structure in which an agent learns a residual policy that adjusts or refines the actions of a pre-existing base controller, allowing for improved performance and adaptability. Trumpp et al. (2023) introduced a residual policy learning approach specifically for **AR** in simulation. Their method involved training the residual policy to adjust a base **Pure Pursuit (PP)** controller’s actions and demonstrated to be effective in high-speed racing tasks by reducing lap times and enhancing stability when evaluated on simulated **F1TENTH** racing tracks. Ghignone et al. (2025) deployed a similar approach on the physical **F1TENTH** platform. Such an agent, trained in simulation, was then able to improve the lap time of the base controller with the help of an **RL** policy. However, the achieved lap times were still significantly slower than **SotA** classical algorithms. In this work, the residual **RL** approach is adopted due to its faster convergence to fast lap times, essential for achieving on-board learning with limited time.

On-Robot learning eliminates the **sim-to-real** gap entirely by training directly on physical robots but needs particularly efficient structures to achieve high performance (Wu et al., 2023), as the massively parallel architectures that are available in simulation (Rudin et al., 2021) are often not replicable. Some works have been developed directly on-board, such as in Bosello et al. (2022), where an agent could successfully navigate an oval track with three hours of training, relying solely on **Light Detection And Ranging (LiDAR)** scans for its observations. The final policy achieved speeds of approximately 2 m/s. Similarly, Evans et al. (2023b) trained an agent under the supervision of a safety system based on a viability kernel designed to ensure crash-free operation. With this setup, the agent outperformed a simulation-trained baseline in terms of lap times and reliability, achieving efficient training within 10 min. However, the approach was constrained by a speed limit of 2 m/s and required the vehicle to pause every 20 steps to update the policy, highlighting areas for improvement in achieving uninterrupted, high-speed training. FastRLAP (Stachowicz et al., 2023)

introduced an online RL framework for AR, achieving stable driving behavior within 20 min of real-world training with an image-to-action approach. However, the approach required an external workstation for policy updates, constraining its scalability and applicability in resource-constrained environments, and was limited to speeds up to 4.5 m/s. Pan et al. (2020) used imitation learning on a scaled car to match an MPC expert used to generate data. However, this approach did not surpass the SotA performance and depended on image-to-action methods and an onboard Graphical Processing Unit (GPU).

In contrast to the previous work, our contribution consistently surpasses the SotA AR agents, both with and without the residual structure, and displays agile racing, without any speed limitation and reaching over 6.5 m s^{-1} . Similarly to other algorithms, our algorithm needs around 20 min of training, but it only trains locally (on the scaled autonomous platform) and with no access to a GPU. Finally, our proposed solution is validated on a real platform across multiple track configurations and tire conditions, highlighting the empirical robustness of the method.

3 Methodology

The residual control architecture utilized throughout this work is illustrated in Figure 1. Detailed descriptions of each block are given in the subsequent sections.

This study is conducted and validated on the FITENTH platform (O’Kelly et al., 2020), a scaled racing platform with form factor 1:10. Localization and state estimation on a mapped track layout is based on a Simultaneous Localization and Mapping (SLAM) system using a 2D LiDAR sensor and Inertial Measurement Unit (IMU). The hardware setup, software architecture (implemented using the Robot Operating System (ROS)), and the localization pipeline closely replicate the approach outlined in Baumann et al. (2024). All computations are conducted on the onboard Intel i7-10710U processor.

3.1 State Machine

To facilitate efficient and autonomous training without human intervention, a state machine is implemented to recover the vehicle from terminal states. Two terminal states are defined: the first occurs when a track-boundary violation is detected, which happens if the center of the rear axle moves outside the defined track boundaries. The second terminal state is triggered by the intervention of the relative-heading safety filter, as detailed in the subsequent section.

Upon reaching a terminal state, the RL agent is deactivated and the baseline controller steers the car back to the reference trajectory. Once the vehicle orientation realigns with the reference trajectory, a new learning episode is initiated, and the residual controller resumes operation. This process ensures seamless episode transitions and continuous data collection, enabling stable and efficient training.

3.2 Curriculum Safety Filter

A relative-heading safety filter is implemented to prevent the vehicle from leaving the track with a large relative heading, Δ , with respect to the reference trajectory. The safety filter signals a terminal state if $j\Delta_j > \Delta_{\text{filter}}$, where $\Delta = \theta - \theta_{\text{ref}}$, θ is the vehicle’s current heading, and θ_{ref} is the heading of the reference trajectory in the global frame. The safety filter is implemented with an adaptive threshold, Δ_{filter} . If the agent completes a lap successfully, Δ_{filter} is increased by δ ; conversely, it is decreased by the same amount if a track-boundary violation is detected.

This mechanism serves two purposes: first, it prevents the vehicle from traversing the run-off area with a heading towards the physical barriers, giving the state machine more time to intervene. Second, it facilitates the agent’s learning process by acting as a curriculum mechanism (Bengio et al., 2009), forcing it to follow the reference trajectory more closely in the beginning, before relaxing the constraint.

3.3 Action Space

The control command is defined as $u = [\delta; v]^T$, where δ is the steering angle, and v the velocity. The command is the sum of the base controller’s output, $u_{\text{base}} = [\delta_{\text{base}}; v_{\text{base}}]^T$, and the **RL** controller’s output, $u_{\text{RL}} = [\delta_{\text{RL}}; v_{\text{RL}}]^T$.

The base controller operates within the ranges $\delta_{\text{base}} \in [0.42; 0.42]$ rad and $v_{\text{base}} \in [0; 10]$ m/s. The learned policy refines u_{base} with residual adjustments, constrained to $\delta_{\text{RL}} \in [0.15; 0.15]$ rad and $v_{\text{RL}} \in [0.5; 2]$ m/s. This formulation allows the residual controller to make fine adjustments to the base controller’s output, enabling greater adaptability, precision, and ultimately faster lap times.

3.4 Observation Space

All observations are based on the onboard state estimation. The observation space is constructed similarly to Ghignone et al. (2024), incorporating vehicle state, dynamics, and track information. The vehicle dynamics and state are represented by $o_{\text{car}} = [v_x; v_y; \dot{\psi}; \Delta d; \Delta \psi; \delta_{\text{base}}; v_{\text{base}}; \delta_{\text{RL,prev}}; v_{\text{RL,prev}}]^T$, where v_x and v_y are the lateral and longitudinal velocities in the car frame, $\dot{\psi}$ is the yaw rate, Δd is the car’s lateral deviation from the reference line, and $\Delta \psi$ is its relative heading to the reference line. δ_{base} and v_{base} are the outputs of the base controller, and $\delta_{\text{RL,prev}}$ and $v_{\text{RL,prev}}$ are the outputs of the **RL** controller of the previous time step.

To capture track information, the observation space includes o_{track} , which summarizes the upcoming reference trajectory and track boundaries. A total of J equally spaced points along the reference trajectory are sampled within a horizon of l meters. At each sampled point, the positions of the reference line, left boundary, and right boundary are stored in the car frame. Formally, this is expressed as $o_{\text{track}} = [\mathbf{p}_{\text{ref}}^0; \dots; \mathbf{p}_{\text{ref}}^J; \mathbf{p}_{\text{left}}^0; \dots; \mathbf{p}_{\text{left}}^J; \mathbf{p}_{\text{right}}^0; \dots; \mathbf{p}_{\text{right}}^J]^T$, where $\mathbf{p}_{\text{ref}} \in \mathbb{R}^2$ represents a two-dimensional point on the race line, and \mathbf{p}_{left} and $\mathbf{p}_{\text{right}}$ represent points on the left and right track boundaries, respectively. The complete observation space is then defined as $o = [o_{\text{car}}; o_{\text{track}}]^T$, with $o \in \mathbb{R}^{5+6J}$ and is normalized. A graphical representation of the observation space is available in the supplementary material, Figure 7.

3.5 Reward Function

The reward consists of a positive term Δs , granted at every step for progress along the reference line Δs and scaled by the constant β (Chisari et al., 2021; Ghignone et al., 2024), as well as a negative penalty ρ , applied only upon track-boundary violations or safety filter interventions. Both terms are mutually exclusive.

Track-boundary violations and safety filter interventions both trigger a state reset: on the physical platform the reset is handled by yielding control solely to the baseline controller until the car has returned within 10 cm of the race line. An additional second is then waited, before the **RL** inputs are applied again. In the case of the **Follow the Gap (FTG)** controller, only the one second timer is applied.

3.6 Training Architecture

To improve data efficiency, we extend **SAC** (Haarnoja et al., 2018) from Stable Baselines (Hill et al., 2018) with an asynchronous pipeline that separates the agent into an acting policy actor and a training policy, akin to *Async-SAC-1* from Yuan & Mahmood (2022). Then the proposed approach incorporates multi-step **TD** learning (Sutton & Barto, 2018), similarly to previous **AR** work (Vasco et al., 2024), to stabilize training (Barth-Maron et al., 2018).

Additionally, a **HDRA** mechanism, inspired by principles from **HER** (Andrychowicz et al., 2017) and reward shaping (Ng et al., 1999), has been adopted and integrated. In scenarios where the agent reaches a terminal state with a negative reward, the N most recent transitions in the replay buffer are retroactively modified to amplify the penalty and create a stronger learning signal to discourage

failure and the actions leading up to it. The stored rewards are then adjusted as follows: given an index $i_{term} \in \mathbb{N}$ corresponding to a terminal state stored in the replay buffer, the reward associated with the action that led to this state is $r_{i_{term}-1} = \rho$. The N previous rewards (r^{old}) are then decreased with a linearly decreasing term as follows:

$$r_{i_{term}-1-j} = r_{i_{term}-1-j}^{old} - \frac{N-j}{N}\rho; \quad \forall j \in [0; 1; \dots; N-1]; \quad (1)$$

The corresponding pseudocode is attached in Appendix G.

During training, the control frequency of the residual RL controller is set to 10 Hz, with the training policy updated at 32 Hz and the behavior policy synced with the latter at 1 Hz. During deployment, the control frequency is increased to 15 Hz, while the baseline controllers operate at a fixed frequency of 40 Hz throughout both training and deployment phases. The output of the RL controller is continually added to the output of the base controller.

4 Experimental Setup

The effectiveness and robustness of the proposed architecture are evaluated through a series of time-trial experiments. The primary objective is to minimize lap time while maintaining stability and reliability over multiple laps. Each scenario is allocated a single 5000 mA h battery for training, which lasts between 20 and 33 min depending on the track-tire configuration and speed profile. After training, the agent is deployed until it completes 20 laps without track-boundary violations. Metrics such as lap times and number of boundary violations are recorded to evaluate speed, repeatability, and adaptability.

4.1 Evaluation

One of the most important goals of this evaluation is to demonstrate the generalization of the proposed approach. This is done by integrating the residual RL controller with three distinct baseline controllers (PP, Model and Acceleration-Based Pursuit (MAP), and FTG, as detailed in Section 4.2) and by testing it in an E2E configuration. Each configuration was evaluated on the 41 m long C-track, with performance measured by the minimum lap time over 20 consecutive deployment laps.

Following these initial experiments, the best-performing combination was selected for further evaluation. These extended tests included repeated training and deployment with varying random seeds on the C-track and on the 34 m long Y-track to assess repeatability and robustness. While these primary experiments were conducted using Turbo tires with a relatively high static friction coefficient of $\frac{\mu_{Turbo}}{\mu_{static}} = 1.01$, additional experiments were performed on the C-track using Thermo-plastic Polyurethane (TPU) tires, which exhibit a lower static friction coefficient of $\frac{\mu_{TPU}}{\mu_{static}} = 0.75$ and different cornering behavior. This allowed for a comprehensive analysis of the controller's performance under varying track and tire conditions. Images of the F1TENTH car, tires, and track setup can be seen in Appendix B.

4.2 Baselines

The following baseline controllers are used to evaluate the agent's learning enhancements and integration capabilities with different baseline controllers:

PP: A classical geometric controller that calculates steering based on a look-ahead point on a pre-defined reference trajectory. This controller operates under a no-slip assumption, making it limited at high speeds where friction dynamics become significant (Coulter, 1992).

Model and Acceleration-Based Pursuit (MAP): An extended pursuit method that integrates a lookup table to incorporate tire dynamics, allowing for improved handling in high-speed corners by accounting for non-linear friction effects (Becker et al., 2023).

Follow the Gap (FTG): This reactive approach identifies gaps in the LiDAR measurements to navigate through (Sezer & Gokasan, 2012). Therefore, it is often the chosen controller when navigating unknown environments with physical boundaries. However, due to its reactive behavior and lack of knowledge regarding the upcoming track sections, it often lags behind in terms of lap time.

End-to-End (E2E): To demonstrate the data efficiency of the proposed RL architecture and isolate its performance, experiments without a baseline controller are conducted. The range for the commanded steering angle is extended to $[-0.42; 0.42]$ rad, which aligns with the limits of the physical steering actuator. For the commanded speed, a curriculum learning approach has been implemented (Wang et al., 2022). The action space for the speed command is $[0; 5]$ with $\geq [1; 7]$ m/s. v is increased by 0.5 m/s as soon as the agent completes three consecutive laps without track-boundary violation. Naturally, the baseline control command is removed from the observation space.

Remark: While MPC provides precise trajectory tracking and constraint adherence, it is not combined with the residual controller in this study as its constraint-based nature inherently conflicts with RL’s adaptive learning, especially when the agent attempts to operate near the limits of the MPC’s predefined constraints. Nonetheless, we include MPC performance in our baseline evaluation, as it is recognized as one of the most performant controllers in the literature (Vázquez et al., 2020) and provides a valuable reference point for contextualizing our results. More detail on the optimization problem formulation, also derived from the work of Vázquez et al. (2020), is available in Appendix J.

5 Results

Figure 2 shows the lap time improvement during training for the different residual RL controllers and the E2E RL controller on the C-track, highlighting the agent’s ability to improve upon the performance of all baseline controllers. While RL MAP and RL PP outperformed their respective base controller within 10 min, RL FTG needed about 20 min to achieve the same. The E2E agent also shows significant lap time improvements within 20 min, but does not manage to reach the SotA baseline set by the MAP controller.

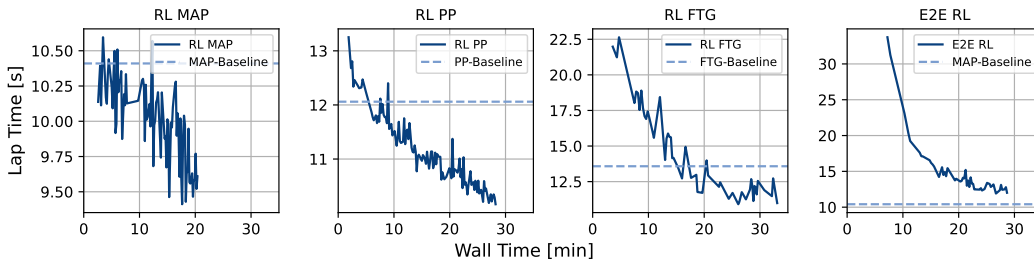


Figure 2: Lap Time vs. Wall Time during training for different residual controllers, with respective reference for best lap time of the baseline controller when available. Additionally, the first 28.8 min of E2E training are shown, compared to the MAP baseline. Only lap times without boundary violations are recorded. Lines start after the first collision-free lap and end when training ends (i.e. when the battery runs out). A unified view of the training lap times is available in Figure 9 for comparison.

During deployment, the RL MAP controller achieved the fastest lap time of 9.26 s, significantly surpassing the MAP baseline’s best of 10.41 s. Across all baseline-residual RL combinations, lap time reductions ranged from 11.0 % to 20.5 % for best lap times and 9.0 % to 20.3 % for mean lap times. An extended table listing all minimum, average and the Standard Deviation (SD) of the lap times for the different combinations can be seen in Appendix C. RL MAP’s superior results in terms of minimum and average lap time made it the primary choice for subsequent experiments.

E2E extended training: Since training the E2E controller for only one battery life was not sufficient to obtain SotA performance, the experiment was extended to three battery lives, cumulating in 82 min of on-track learning. Afterward, the agent’s average lap time was 5.0 % lower than the SotA set by the MAP controller, while the minimum lap time was 7.3 % lower (Extended E2E RL: $t_{min}=9.65$ s, $t =9.97$ s. MAP: $t_{min}=10.41$ s, $t =10.50$ s). During the deployment, only 4 track-bound violations and speeds up to 7 m s^{-1} were registered. Extended data and visualizations of the deployment runs can be seen in Appendix C.

5.1 RL MAP Extended Evaluation

The RL MAP controller was further re-trained from scratch in two different conditions and across three different random seeds to evaluate the method across environments. The first environment consisted of using the more slippery TPU tires on the same track (C-track), while the second experiment evaluated the algorithm on the Y-track. Tires pictures and track layouts are available in Appendix B and Appendix E. The RL MAP controller consistently outperformed its baseline across all scenarios tested, achieving improvements ranging from 5.4% to 11.5% for minimum lap times and 5.9% to 9.0% for mean lap times. Even during the worst deployment run in terms of lap time reduction, the proposed architecture managed to decrease the minimum lap time by 0.57 s and the average lap time by 0.51 s. This highlights the robustness of the approach across varying track layouts, friction levels, and weight initialization of the neural network. Table 1 summarizes the three deployment runs per tire and track combination. A detailed break-down of the individual deployments is presented in the Appendix E.

Ctrl.	C-Track, Turbo				C-Track, TPU				Y-Track, Turbo			
	$t_{min} \downarrow$	$t_{\mu} \downarrow$	$\sigma \downarrow$	$n_b \downarrow$	$t_{min} \downarrow$	$t_{\mu} \downarrow$	$\sigma \downarrow$	$n_b \downarrow$	$t_{min} \downarrow$	$t_{\mu} \downarrow$	$\sigma \downarrow$	$n_b \downarrow$
MPC	11.86	11.95	0.083	0	13.14	13.25	0.179	0	9.97	10.04	0.071	1
MAP	10.41	10.50	0.060	0	12.93	13.45	0.338	0	8.55	8.62	0.045	0
RL MAP (Ours)	9.26	9.56	0.181	2	12.23	12.50	0.163	1	7.57	7.97	0.205	6

Table 1: Performance of RL MAP with different tire-track combinations averaged over three randomly initialized seeds compared to MAP and MPC for reference. t_{min} [s] represents the minimum lap time, t [s] the average lap time, σ [s] the standard deviation of the lap times and n_{bound} the number of boundary violations until 20 violation-free laps are reached.

In terms of lap time repeatability, RL MAP exhibited a more than three times larger lap time standard deviation compared to its baseline controller on the high-friction Turbo tires. However, in the low-friction scenario, RL MAP demonstrated greater consistency with an SD of 0.16 s, producing more stable lap times than its baseline controller with a SD of 0.34 s. While the MAP baseline was capable of completing 20 consecutive laps without any track-boundary violations across all scenarios, the residual agent experienced up to two violations on the C-track with Turbo tires, up to one violation on the C-track with TPU tires, and up to five on the Y-track track before successfully completing 20 violation-free laps. The majority of these violations occurred due to slight corner clipping.

Qualitative observations indicate that the RL MAP controller adjusts steering and speed effectively across the track. For example, on the C-track with Turbo tires (Figure 3) the residual controller negotiates all the corners but one with higher minimum speed, without sacrificing straight speed, as it also reaches higher top velocities at the end of the acceleration sections. Similar behavior can be observed in the other configurations in the supplementary material, Appendix E.

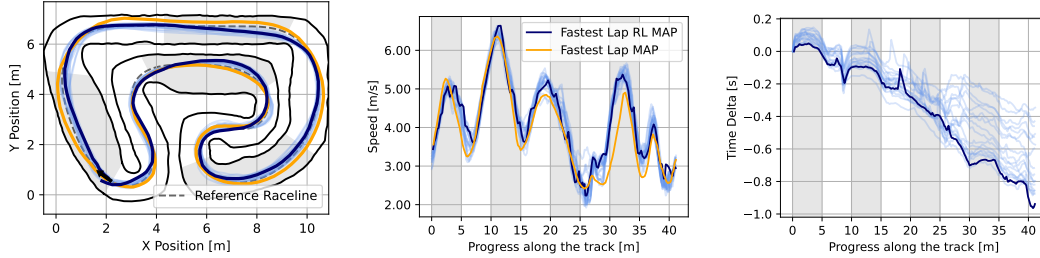


Figure 3: Comparison of the driven trajectories, speed profiles, and the time delta for **RL MAP** (blue) vs. **MAP** (orange) on the C-track with Turbo tires. Speed profiles and time deltas are represented along the positional advancement on the track. The zero progress position corresponds to the black arrow in the bottom left corner, and the track is driven in the sense of the arrow. Dark blue represents the fastest lap of **RL MAP**.

5.2 RL MAP Generalization Evaluation

Generalization to a different track layout was evaluated by deploying an **RL MAP** agent, trained on the C-track with Turbo tires, on the Y-track with same tires using zero-shot (no additional training) and few-shot transfer (additional training for one battery life on the new track).

In zero-shot transfer, the results across random seeds were mixed and not all 20 laps could be completed, with the aggregate deployment attaining $t = 8.68\text{ s}$; $\sigma = 0.34\text{ s}$. While Seed 1 managed to outperform the baseline in terms of best and mean lap times after only one collision, Seed 2 and Seed 3 experienced significant instability, with multiple track-boundary violations that necessitated terminating the deployment.

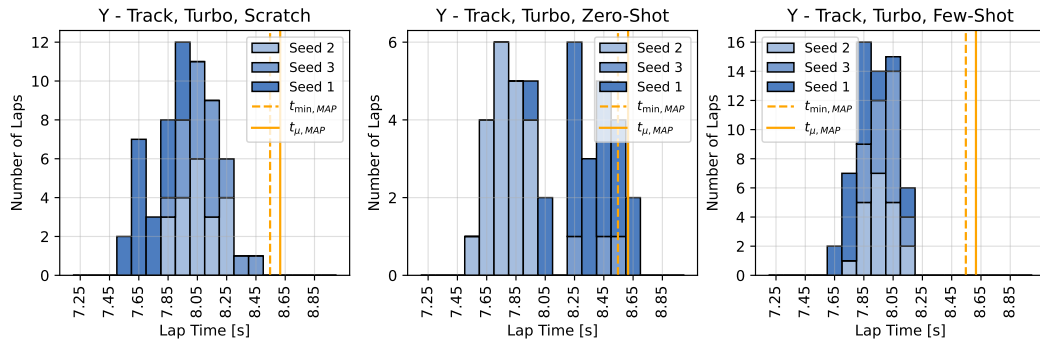


Figure 4: Stacked histogram of lap times achieved during zero-shot and few-shot transfer from the C-track to Y-track during 20 boundary-violation-free laps. Different shades represent the three different weight initialization and resulting policies learned on the C-track.

Due to the very limited zero-shot transfer capabilities of the method, we proceeded to further test few-shot transfer, which involved additional training for one battery life. This led to improvements in both lap repeatability and lap times compared to zero-shot transfer. When compared to policies trained from scratch on the Y-track, the few-shot transfer policy demonstrated fewer track-boundary violations (up to two per seed, four in total), an on average 4.7% lower mean lap time and half the standard deviation in lap times across all random seeds. The aggregate laps demonstrated $t = 7.93\text{ s}$, $\sigma = 0.13\text{ s}$. Figure 4 presents a distribution of all the lap times recorded for the evaluation, highlighting the effectiveness of few-shot transfer in enhancing lap repeatability. Extended results of the generalization tests can be found in Appendix F.

5.3 Ablation Study

We evaluate the impact of key architectural and algorithmic modifications with an ablation study conducted in the real-time F1TENTH ROS simulator (O’Kelly et al., 2019). This study focuses on the more challenging E2E setting, comparing various combinations of multi-step TD learning, HDRA, and training architectures (asynchronous vs. synchronous). Figure 5 presents the results, averaged over five independent training runs with different random seed initializations.

A first comparison shows that in our experiments the asynchronous architecture (HDRA + TD3, Async) manages to reduce the lap times faster than the synchronous architecture (HDRA + TD3, Sync), and in the same training time achieves a faster lap time compared to its synchronous counterpart. This improvement is likely due to the ability of the asynchronous architecture to support a policy update rate three times higher.

Furthermore, the addition of multi-step TD error (TD3, Async), shows in our experiments to help speed up the learning process, achieving lap completions earlier than the ten-minute mark, while (TD1, Async) needs in this case around 20 min. Finally, the addition of HDRA (HDRA + TD3, Async) does not show a statistically relevant improvement against (TD3, Async) in average lap time, but keeps the lap time spread lower, and makes the training more consistent across random seeds. Detailed metrics on the lap times achieved during the last three minutes of training are available in Appendix H.

6 Conclusion

This work presented a real-world on-board learning framework for AR, applied to a residual and E2E control framework. The residual controller consistently improves the performance of its baseline across all tested scenarios, achieving substantial reductions in minimum and average lap times. Among the tested configurations, the RL MAP controller delivers the fastest lap times, improving the minimum lap time by up to 11.5% and the average lap time by up to 10.0% compared to the classical MAP controller. Beyond improved performance, it demonstrates strong repeatability and stability across different tracks and tire configurations, as well as weight initializations. Moreover, the proposed asynchronous framework is highly efficient, reaching said performance within a single battery life of 20 to 33 min (10 k to 19 k environmental steps) for training.

The E2E RL controller further illustrates the versatility of the architecture. After 29 min of training, it navigated the track consistently at speeds up to 4 m s^{-1} and with 82 min of training, surpassed the MAP baseline by over half a second, maintaining stable performance at speeds up to 7 m s^{-1} . The ablation study shows that especially the asynchronous structure and multi-step TD learning attributes to the fast convergence to the minimal lap time.

Furthermore, while the few-shot generalization experiments show that a single policy can be tuned to drive consistently on a different track, the zero-shot experiments show that future work could focus on methods targeting generalization across different real-world conditions. For example, recent work on data-driven simulation (Xiao et al., 2024; Rothfuss et al., 2024) could be a starting point for creating a generalist policy that would then benefit from the framework proposed here for on-board fine-tuning.

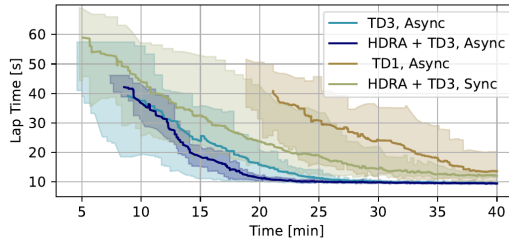


Figure 5: Lap times during training averaged over 5 runs for ablation regarding multi-step TD over one (TD1) and three (TD3) steps, a synchronous (sync) and asynchronous (async) architecture as well as with HDRA and without. Lines only start when the first collision-free lap is completed. The area between the minimum and the maximum lap time is shaded.

Overall, these findings highlight the potential of a residual RL framework to enhance classical controllers, while the same framework enables E2E RL agents to achieve competitive real-world performance. Future research could focus on reducing track-boundary violations during training via a model-based safety filter (Evans et al., 2023a; Tearle et al., 2021) or extending the residual control architecture to multi-agent racing, which would introduce new challenges, such as dynamic collision avoidance and strategic adaptation. Finally, the proposed architecture could be adapted for full-scale vehicles.

Broader Impact Statement

The versatility of the framework also makes it a candidate for other domains, including drone racing, robotic locomotion, and manipulation tasks. In future work, we are considering exploring how these applications could validate this work’s effectiveness in different high-speed or precision-critical scenarios, expanding its relevance to a broader range of autonomous systems.

References

- Marcin Andrychowicz, Filip Wolski, Alex Ray, Jonas Schneider, Rachel Fong, Peter Welinder, Bob McGrew, Josh Tobin, OpenAI Pieter Abbeel, and Wojciech Zaremba. Hindsight Experience Replay. In *Advances in Neural Information Processing Systems*, volume 30. Curran Associates, Inc., 2017.
- Gabriel Barth-Maron, Matthew W. Hoffman, David Budden, Will Dabney, Dan Horgan, Dhruva TB, Alistair Muldal, Nicolas Heess, and Timothy Lillicrap. Distributional policy gradients. In *International Conference on Learning Representations*, 2018. URL <https://openreview.net/forum?id=SyZi pzbCb>.
- Nicolas Baumann, Edoardo Ghignone, Jonas Kühne, Niklas Bastuck, Jonathan Becker, Nadine Imholz, Tobias Kränzlin, Tian Yi Lim, Michael Lötscher, Luca Schwarzenbach, Luca Tognoni, Christian Vogt, Andrea Carron, and Michele Magno. ForzaETH Race Stack – Scaled Autonomous Head-to-Head Racing on Fully Commercial off-the-Shelf Hardware. *Journal of Field Robotics*, 3 2024. ISSN 15564967. DOI: 10.1002/rob.22429.
- Jonathan Becker, Nadine Imholz, Luca Schwarzenbach, Edoardo Ghignone, Nicolas Baumann, and Michele Magno. Model- and Acceleration-based Pursuit Controller for High-Performance Autonomous Racing. In *2023 IEEE International Conference on Robotics and Automation (ICRA)*, pp. 5276–5283, 2023. DOI: 10.1109/ICRA48891.2023.10161472.
- Yoshua Bengio, Jérôme Louradour, Ronan Collobert, and Jason Weston. Curriculum learning. In *Proceedings of the 26th annual international conference on machine learning*, pp. 41–48, 2009.
- Johannes Betz, Tobias Betz, Felix Fent, Maximilian Geisslinger, Alexander Heilmeyer, Leonhard Hermansdorfer, Thomas Herrmann, Sebastian Huch, Phillip Karle, Markus Lienkamp, Boris Lohmann, Felix Nobis, Levent Ögretmen, Matthias Rowold, Florian Sauerbeck, Tim Stahl, Rainer Trauth, Frederik Werner, and Alexander Wischnewski. Tum autonomous motorsport: An autonomous racing software for the indy autonomous challenge. *Journal of Field Robotics*, 40(4): 783–809, 2023. DOI: <https://doi.org/10.1002/rob.22153>. URL <https://onlinelibrary.wiley.com/doi/abs/10.1002/rob.22153>.
- Michael Bosello, Rita Tse, and Giovanni Pau. Train in Austria, Race in Montecarlo: Generalized RL for Cross-Track F1TENTH LIDAR-Based Races. In *2022 IEEE 19th Annual Consumer Communications & Networking Conference (CCNC)*, pp. 290–298, 2022. DOI: 10.1109/CCNC49033.2022.9700730.
- Alberto Broggi, Massimo Bertozzi, Alessandra Fascioli, and Gianni Conte. *Automatic Vehicle Guidance*. WORLD SCIENTIFIC, 1999. DOI: 10.1142/3986.

- Axel Brunnbauer, Luigi Berducci, Andreas Brandstätter, Mathias Lechner, Ramin Hasani, Daniela Rus, and Radu Grosu. Latent Imagination Facilitates Zero-Shot Transfer in Autonomous Racing. In *2022 International Conference on Robotics and Automation (ICRA)*, pp. 7513–7520, 2022. DOI: 10.1109/ICRA46639.2022.9811650.
- Eugenio Chisari, Alexander Liniger, Alisa Rupenyan, Luc Van Gool, and John Lygeros. Learning from simulation, racing in reality. In *2021 IEEE International Conference on Robotics and Automation (ICRA)*, pp. 8046–8052. IEEE, 2021.
- RC Coulter. Implementation of the Pure Pursuit Path Tracking Algorithm. *DTIC Document*, 1992.
- Marc Peter Deisenroth and Carl Edward Rasmussen. Pilco: a model-based and data-efficient approach to policy search. In *Proceedings of the 28th International Conference on International Conference on Machine Learning, ICML'11*, pp. 465–472, Madison, WI, USA, 2011. Omnipress. ISBN 9781450306195.
- Onur Dikici, Edoardo Ghignone, Cheng Hu, Nicolas Baumann, Lei Xie, Andrea Carron, Michele Magno, and Matteo Corno. Learning-based on-track system identification for scaled autonomous racing in under a minute. *IEEE Robotics and Automation Letters*, 10(2):1984–1991, 2025. DOI: 10.1109/LRA.2025.3527336.
- Benjamin D. Evans, Hendrik W. Jordaan, and Herman A. Engelbrecht. Safe reinforcement learning for high-speed autonomous racing. *Cognitive Robotics*, 3:107–126, 2023a. ISSN 2667-2413. DOI: <https://doi.org/10.1016/j.cogr.2023.04.002>.
- Benjamin David Evans, Johannes Betz, Hongrui Zheng, Herman A. Engelbrecht, Rahul Mangharam, and Hendrik W. Jordaan. Bypassing the Simulation-to-Reality Gap: Online Reinforcement Learning Using a Supervisor. In *2023 21st International Conference on Advanced Robotics (ICAR)*, pp. 325–331, 2023b. DOI: 10.1109/ICAR58858.2023.10406465.
- Benjamin David Evans, Herman Arnold Engelbrecht, and Hendrik Willem Jordaan. High-Speed Autonomous Racing Using Trajectory-Aided Deep Reinforcement Learning. *IEEE Robotics and Automation Letters*, 8(9):5353–5359, 2023c. DOI: 10.1109/LRA.2023.3295252.
- Benjamin David Evans, Hendrik Willem Jordaan, and Herman Arnold Engelbrecht. Comparing deep reinforcement learning architectures for autonomous racing. *Machine Learning with Applications*, 14:100496, 2023d. ISSN 2666-8270. DOI: <https://doi.org/10.1016/j.mlwa.2023.100496>.
- Florian Fuchs, Yunlong Song, Elia Kaufmann, Davide Scaramuzza, and Peter Durr. Super-Human Performance in Gran Turismo Sport Using Deep Reinforcement Learning. *IEEE Robotics and Automation Letters*, 6:4257–4264, 7 2021. ISSN 23773766. DOI: 10.1109/LRA.2021.3064284.
- Edoardo Ghignone, Nicolas Baumann, and Michele Magno. Tc-driver: A trajectory-conditioned reinforcement learning approach to zero-shot autonomous racing. *IEEE Transactions on Field Robotics*, 1:527–536, 2024. DOI: 10.1109/TFR.2024.3499912.
- Edoardo Ghignone, Nicolas Baumann, Cheng Hu, Jonathan Wang, Lei Xie, Andrea Carron, and Michele Magno. Rlpp: A residual method for zero-shot real-world autonomous racing on scaled platforms, 2025. URL <https://arxiv.org/abs/2501.17311>.
- Ross Girshick, Jeff Donahue, Trevor Darrell, and Jitendra Malik. Region-Based Convolutional Networks for Accurate Object Detection and Segmentation. *IEEE Transactions on Pattern Analysis and Machine Intelligence*, 38(1):142–158, 2016. DOI: 10.1109/TPAMI.2015.2437384.
- Sorin Grigorescu, Bogdan Trasnea, Tiberiu Cocias, and Gigel Macesanu. A survey of deep learning techniques for autonomous driving. *Journal of Field Robotics*, 37(3):362–386, 2020. DOI: <https://doi.org/10.1002/rob.21918>.

- Tuomas Haarnoja, Aurick Zhou, Pieter Abbeel, and Sergey Levine. Soft Actor-Critic: Off-Policy Maximum Entropy Deep Reinforcement Learning with a Stochastic Actor. In Jennifer Dy and Andreas Krause (eds.), *Proceedings of the 35th International Conference on Machine Learning*, volume 80 of *Proceedings of Machine Learning Research*, pp. 1861–1870. PMLR, 10–15 Jul 2018.
- Danijar Hafner, Jurgis Pasukonis, Jimmy Ba, and Timothy P. Lillicrap. Mastering diverse domains through world models. *CoRR*, abs/2301.04104, 2023. URL <https://doi.org/10.48550/arXiv.2301.04104>.
- Alexander Heilmeier, Alexander Wischnewski, Leonhard Hermansdorfer, Johannes Betz, Markus Lienkamp, and Boris Lohmann. Minimum curvature trajectory planning and control for an autonomous race car. *Vehicle System Dynamics*, 58(10):1497–1527, 10 2020. ISSN 0042-3114. DOI: 10.1080/00423114.2019.1631455.
- Ashley Hill, Antonin Raffin, Maximilian Ernestus, Adam Gleave, Anssi Kanervisto, Rene Traore, Prafulla Dhariwal, Christopher Hesse, Oleg Klimov, Alex Nichol, Matthias Plappert, Alec Radford, John Schulman, Szymon Sidor, and Yuhuai Wu. Stable Baselines. <https://github.com/hill-a/stable-baselines>, 2018.
- David Hoeller, Nikita Rudin, Dhionis Sako, and Marco Hutter. Anymal parkour: Learning agile navigation for quadrupedal robots. *Science Robotics*, 9(88):eadi7566, 2024. DOI: 10.1126/scirobotics.adi7566. URL <https://www.sciencemag.org/doi/abs/10.1126/scirobotics.adi7566>.
- Michael Janner, Justin Fu, Marvin Zhang, and Sergey Levine. When to trust your model: Model-based policy optimization. In H. Wallach, H. Larochelle, A. Beygelzimer, F. d'Alché-Buc, E. Fox, and R. Garnett (eds.), *Advances in Neural Information Processing Systems*, volume 32. Curran Associates, Inc., 2019. URL https://proceedings.neurips.cc/paper_files/paper/2019/file/5faf461eff3099671ad63c6f3f094f7f-Paper.pdf.
- Tobias Johannink, Shikhar Bahl, Ashvin Nair, Jianlan Luo, Avinash Kumar, Matthias Loskyll, Juan Aparicio Ojea, Eugen Solowjow, and Sergey Levine. Residual reinforcement learning for robot control. In *2019 international conference on robotics and automation (ICRA)*, pp. 6023–6029. IEEE, 2019.
- Elia Kaufmann, Leonard Bauersfeld, Antonio Loquercio, Matthias Müller, Vladlen Koltun, and Davide Scaramuzza. Champion-level drone racing using deep reinforcement learning. *Nature*, 620(7976):982–987, 2023.
- Alex H. Lang, Sourabh Vora, Holger Caesar, Lubing Zhou, Jiong Yang, and Oscar Beijbom. PointPillars: Fast Encoders for Object Detection From Point Clouds. In *Proceedings of the IEEE/CVF Conference on Computer Vision and Pattern Recognition (CVPR)*, June 2019.
- Wei Liu, Dragomir Anguelov, Dumitru Erhan, Christian Szegedy, Scott Reed, Cheng-Yang Fu, and Alexander C. Berg. SSD: Single Shot MultiBox Detector. In *Computer Vision – ECCV 2016*, pp. 21–37, Cham, 2016. Springer International Publishing. ISBN 978-3-319-46448-0.
- Andrew Y. Ng, Daishi Harada, and Stuart J. Russell. Policy invariance under reward transformations: Theory and application to reward shaping. In *Proceedings of the Sixteenth International Conference on Machine Learning, ICML '99*, pp. 278–287, San Francisco, CA, USA, 1999. Morgan Kaufmann Publishers Inc. ISBN 1558606122.
- Matthew O’Kelly, Varundev Sukhil, Houssam Abbas, Jack Harkins, Chris Kao, Yash Vardhan Pant, Rahul Mangharam, Dipshil Agarwal, Madhur Behl, Paolo Burgio, and Marko Bertogna. F1/10: An Open-Source Autonomous Cyber-Physical Platform. *ArXiv*, abs/1901.08567, 2019. URL <https://api.semanticscholar.org/CorpusID:59222730>.

- Matthew O'Kelly, Hongrui Zheng, Dhruv Karthik, and Rahul Mangharam. F1TENTH: An Open-source Evaluation Environment for Continuous Control and Reinforcement Learning. In *Proceedings of the NeurIPS 2019 Competition and Demonstration Track*, volume 123 of *Proceedings of Machine Learning Research*, pp. 77–89. PMLR, 08–14 Dec 2020.
- Hans B. Pacejka. Chapter 1 - tire characteristics and vehicle handling and stability. In Hans B. Pacejka (ed.), *Tire and Vehicle Dynamics (Third Edition)*, pp. 1–58. Butterworth-Heinemann, Oxford, third edition edition, 2012. ISBN 978-0-08-097016-5. DOI: <https://doi.org/10.1016/B978-0-08-097016-5.00001-2>. URL <https://www.sciencedirect.com/science/article/pii/B9780080970165000012>.
- Yunpeng Pan, Ching-An Cheng, Kamil Saigol, Keuntaek Lee, Xinyan Yan, Evangelos A Theodorou, and Byron Boots. Imitation learning for agile autonomous driving. *The International Journal of Robotics Research*, 39(2-3):286–302, 2020.
- Xue Bin Peng, Marcin Andrychowicz, Wojciech Zaremba, and Pieter Abbeel. Sim-to-real transfer of robotic control with dynamics randomization. In *2018 IEEE international conference on robotics and automation (ICRA)*, pp. 3803–3810. IEEE, 2018.
- Joseph Redmon, Santosh Divvala, Ross Girshick, and Ali Farhadi. You Only Look Once: Unified, Real-Time Object Detection. In *Proceedings of the IEEE Conference on Computer Vision and Pattern Recognition (CVPR)*, June 2016.
- Jonas Rothfuss, Bhavya Sukhija, Lenart Treven, Florian Dörfler, Stelian Coros, and Andreas Krause. Bridging the sim-to-real gap with bayesian inference. In *2024 IEEE/RSJ International Conference on Intelligent Robots and Systems (IROS)*, pp. 10784–10791, 2024. DOI: 10.1109/IROS58592.2024.10801505.
- Nikita Rudin, David Hoeller, Philipp Reist, and Marco Hutter. Learning to walk in minutes using massively parallel deep reinforcement learning. In *5th Annual Conference on Robot Learning*, 2021. URL <https://openreview.net/forum?id=wK2fDDJ5VcF>.
- Volkan Sezer and Metin Gokasan. A novel obstacle avoidance algorithm: "Follow the Gap Method". *Robotics and Autonomous Systems*, 60(9):1123–1134, September 2012. ISSN 0921-8890. DOI: 10.1016/j.robot.2012.05.021.
- Martin Simony, Stefan Milzy, Karl Amendey, and Horst-Michael Gross. Complex-YOLO: An Euler-Region-Proposal for Real-time 3D Object Detection on Point Clouds. In *Proceedings of the European Conference on Computer Vision (ECCV) Workshops*, September 2018.
- Yunlong Song, Angel Romero, Matthias Müller, Vladlen Koltun, and Davide Scaramuzza. Reaching the limit in autonomous racing: Optimal control versus reinforcement learning. *Science Robotics*, 8(82):eadg1462, 2023. DOI: 10.1126/scirobotics.adg1462. URL <https://www.sciencedirect.com/doi/abs/10.1126/scirobotics.adg1462>.
- Nitish Sontakke, Hosik Chae, Sangjoon Lee, Tianle Huang, Dennis W. Hong, and Sehoon Hal. Residual physics learning and system identification for sim-to-real transfer of policies on buoyancy assisted legged robots. In *2023 IEEE/RSJ International Conference on Intelligent Robots and Systems (IROS)*, pp. 392–399, 2023. DOI: 10.1109/IROS55552.2023.10342062.
- Kyle Stachowicz, Dhruv Shah, Arjun Bhorkar, Ilya Kostrikov, and Sergey Levine. FastRLAP: A System for Learning High-Speed Driving via Deep RL and Autonomous Practicing. In *Proceedings of The 7th Conference on Robot Learning*, volume 229 of *Proceedings of Machine Learning Research*, pp. 3100–3111. PMLR, 06–09 Nov 2023.
- Richard S. Sutton and Andrew G. Barto. *Reinforcement Learning: An Introduction*. The MIT Press, second edition, 2018. URL <http://incompleteideas.net/book/the-book-2nd.html>.

- Ben Tearle, Kim P. Wabersich, Andrea Carron, and Melanie N. Zeilinger. A Predictive Safety Filter for Learning-Based Racing Control. *IEEE Robotics and Automation Letters*, 6(4):7635–7642, 2021. DOI: 10.1109/LRA.2021.3097073.
- C. Thorpe, M.H. Hebert, T. Kanade, and S.A. Shafer. Vision and navigation for the Carnegie-Mellon Navlab. *IEEE Transactions on Pattern Analysis and Machine Intelligence*, 10(3):362–373, 1988. DOI: 10.1109/34.3900.
- Sebastian Thrun, Mike Montemerlo, Hendrik Dahlkamp, David Stavens, Andrei Aron, James Diebel, Philip Fong, John Gale, Morgan Halpenny, Gabriel Hoffmann, Kenny Lau, Celia Oakley, Mark Palatucci, Vaughan Pratt, Pascal Stang, Sven Strohband, Cedric Dupont, Lars-Erik Jendrossek, Christian Koelen, Charles Markey, Carlo Rummel, Joe van Niekerk, Eric Jensen, Philippe Alessandrini, Gary Bradski, Bob Davies, Scott Ettinger, Adrian Kaehler, Ara Nefian, and Pamela Mahoney. Stanley: The robot that won the DARPA Grand Challenge. *Journal of Field Robotics*, 23(9):661–692, 2006. DOI: <https://doi.org/10.1002/rob.20147>.
- Josh Tobin, Rachel Fong, Alex Ray, Jonas Schneider, Wojciech Zaremba, and Pieter Abbeel. Domain randomization for transferring deep neural networks from simulation to the real world. *2017 IEEE/RSJ International Conference on Intelligent Robots and Systems (IROS)*, pp. 23–30, 2017.
- Raphael Trumpp, Denis Hoornaert, and Marco Caccamo. Residual Policy Learning for Vehicle Control of Autonomous Racing Cars. In *2023 IEEE Intelligent Vehicles Symposium (IV)*, pp. 1–6, 2023. DOI: 10.1109/IV55152.2023.10186744.
- Miguel Vasco, Takuma Seno, Kenta Kawamoto, Kaushik Subramanian, Peter R. Wurman, and Peter Stone. A Super-human Vision-based Reinforcement Learning Agent for Autonomous Racing in Gran Turismo. *Reinforcement Learning Journal*, 4:1674–1710, 2024.
- Robin Verschueren, Gianluca Frison, Dimitris Kouzoupis, Jonathan Frey, Niels van Duijkeren, Andrea Zanelli, Branimir Novoselnik, Thivaharan Albin, Rien Quirynen, and Moritz Diehl. acados – a modular open-source framework for fast embedded optimal control. *Mathematical Programming Computation*, 2021.
- José L. Vázquez, Marius Brühlmeier, Alexander Liniger, Alisa Rupenyan, and John Lygeros. Optimization-based hierarchical motion planning for autonomous racing. In *2020 IEEE/RSJ International Conference on Intelligent Robots and Systems (IROS)*, pp. 2397–2403, 2020. DOI: 10.1109/IROS45743.2020.9341731.
- Xin Wang, Yudong Chen, and Wenwu Zhu. A Survey on Curriculum Learning. *IEEE Transactions on Pattern Analysis and Machine Intelligence*, 44(9):4555–4576, 2022. DOI: 10.1109/TPAMI.2021.3069908.
- Philipp Wu, Alejandro Escontrela, Danijar Hafner, Pieter Abbeel, and Ken Goldberg. DayDreamer: World Models for Physical Robot Learning. In Karen Liu, Dana Kulic, and Jeff Ichnowski (eds.), *Proceedings of The 6th Conference on Robot Learning*, volume 205 of *Proceedings of Machine Learning Research*, pp. 2226–2240. PMLR, 14–18 Dec 2023.
- Wenli Xiao, Haoru Xue, Tony Tao, Dvij Kalaria, John M. Dolan, and Guanya Shi. Anycar to anywhere: Learning universal dynamics model for agile and adaptive mobility, 2024. URL <https://arxiv.org/abs/2409.15783>.
- Yufeng Yuan and A. Rupam Mahmood. Asynchronous Reinforcement Learning for Real-Time Control of Physical Robots. In *2022 International Conference on Robotics and Automation (ICRA)*, pp. 5546–5552, 2022. DOI: 10.1109/ICRA46639.2022.9811771.
- Yang Zhang, Zixiang Zhou, Philip David, Xiangyu Yue, Zerong Xi, Boqing Gong, and Hassan Foroosh. PolarNet: An Improved Grid Representation for Online LiDAR Point Clouds Semantic Segmentation. In *Proceedings of the IEEE/CVF Conference on Computer Vision and Pattern Recognition (CVPR)*, June 2020.

Jingyuan Zhao, Wenyi Zhao, Bo Deng, Zhenghong Wang, Feng Zhang, Wenxiang Zheng, Wanke Cao, Jinrui Nan, Yubo Lian, and Andrew F. Burke. Autonomous driving system: A comprehensive survey. *Expert Systems with Applications*, 242:122836, 2024. ISSN 0957-4174. DOI: <https://doi.org/10.1016/j.eswa.2023.122836>.

Wenshuai Zhao, Jorge Peña Queralta, and Tomi Westerlund. Sim-to-Real Transfer in Deep Reinforcement Learning for Robotics: a Survey. In *2020 IEEE Symposium Series on Computational Intelligence (SSCI)*, pp. 737–744, 2020. DOI: 10.1109/SSCI47803.2020.9308468.

Qin Zou, Qin Sun, Long Chen, Bu Nie, and Qingquan Li. A Comparative Analysis of LiDAR SLAM-Based Indoor Navigation for Autonomous Vehicles. *IEEE Transactions on Intelligent Transportation Systems*, 23(7):6907–6921, 2022. DOI: 10.1109/TITS.2021.3063477.

Supplementary Materials

The following content was not necessarily subject to peer review.

A Extended Related Works

Autonomous driving research has evolved significantly, from early experiments in the 1970s to today's sophisticated systems. [Zhao et al. \(2024\)](#) provide a comprehensive overview of these advancements, highlighting the field's interdisciplinary nature. Foundational projects like the NavLab series ([Thorpe et al., 1988](#)) and the ARGO vehicle ([Broggi et al., 1999](#)) laid the groundwork for integrating technologies such as computer vision, machine learning, and advanced sensor systems into autonomous systems. These pioneering efforts were further accelerated by the DARPA Grand Challenges in 2004 and 2005, which catalyzed the adoption of machine learning and data-driven methods in autonomous vehicle development, driving the transition to computer-controlled vehicles with enhanced autonomy and intelligence ([Thrun et al., 2006](#)).

Various architectures have since been explored in autonomous driving. Layered architectures, with their modular design, excel in reliability and debugging, while end-to-end systems streamline processing through neural networks, though they face challenges related to data dependency and interpretability ([Grigorescu et al., 2020](#)). Significant progress has also been made in perception technologies. For example, Region-based Convolutional Neural Networks ([Girshick et al., 2016](#)) and single-stage methods like [You Only Look Once \(YOLO\)](#) and the [Single-Shot Detector \(SSD\)](#) have revolutionized image-based object detection ([Redmon et al., 2016](#); [Liu et al., 2016](#)). Similarly, advancements in LiDAR-based systems, including [Complex-YOLO](#) and [PointPillars](#), have enhanced 3D perception, critical for real-time navigation and obstacle avoidance ([Simony et al., 2018](#); [Lang et al., 2019](#); [Zhang et al., 2020](#)).

The evolution of [SLAM](#) systems underscores the increasing emphasis on accurate and efficient localization and mapping. Diverse projects demonstrate how vision-based techniques combined with inertial navigation improve robustness across diverse environments ([Zou et al., 2022](#)).

While autonomous driving technologies have matured for structured environments, recent research has shifted towards more dynamic domains like [AR](#). This transition necessitates not only robust perception and planning but also advanced control algorithms capable of operating at the limits of vehicle dynamics. Classical control methods, such as [PP](#) and [MPC](#), have served as reliable baselines. However, [RL](#) has emerged as a promising paradigm, offering superior adaptability and agility for racing tasks.

Reinforcement Learning in Simulation

In high-fidelity simulators like Gran Turismo, [RL](#) has demonstrated exceptional performance. For instance, [Fuchs et al. \(2021\)](#) and [Vasco et al. \(2024\)](#) outperformed human drivers using [SAC](#) and multi-step [TD](#) learning. While [Fuchs et al. \(2021\)](#) employed an observation space similar to ours, [Vasco et al. \(2024\)](#) incorporated a front-facing camera stream. By leveraging an asymmetric [SAC](#) architecture, their approach relied on proprioceptive observations during deployment, excluding information about upcoming track sections. Despite its success in simulation, this method has not yet demonstrated effective real-world transferability.

While [RL](#) methods often outperform classical approaches also in the F1TENTH simulator, this performance fails to transfer to physical environments due to the [sim-to-real](#) gap, as highlighted in the works of [Evans et al. \(2023d\)](#). Factors such as model mismatch, sensor noise, and hardware delays exacerbate this gap, leading to instability and erratic behaviors in real-world deployments. Agents that outperformed a [PP](#) controller in simulation displayed rapid side-to-side swerving and instability during real-world tests, reaching lower speeds and ultimately lower lap times. These findings underscore the persistent challenges of [sim-to-real](#) transfer for [RL](#)-based autonomous racing systems.

Trajectory-Aided Reinforcement Learning

Trajectory-aided RL combines classical trajectory planning with RL to enhance safety, stability, and performance in high-speed racing. Methods such as those proposed by Ghignone et al. (2024) and Evans et al. (2023c) enforce adherence to precomputed trajectories by penalizing deviations. In contrast, our approach primarily uses trajectory information to inform the RL agent about upcoming track sections and define progress along the track, balancing flexibility and control in dynamic environments.

Model-Based Reinforcement Learning Model-based RL has been always well regarded for its sample efficiency, first demonstrated by Deisenroth & Rasmussen (2011) and more recently in the Model Based Policy Optimization (MBPO) (Janner et al., 2019) and Dreamer (Hafner et al., 2023) architectures. Both these methods were shown to work well in real-world tasks, such as for drifting maneuvers (Rothfuss et al., 2024), for locomotion and navigation (Wu et al., 2023), and on the F1TENTH platform, where Brunnbauer et al. (2022) applied Dreamer to achieve faster lap times in simulation compared to model-free methods. However, this last application exhibited bang-bang control behavior when transferred to the real world, resulting in suboptimal performance. Additionally, model-based methods require high computational demands and external workstations, making this solution unsuitable for fully on-board learning on resource-constrained platforms like the F1TENTH one, highlighting the need for more efficient on-car learning methods.

B Experimental Setup

Figure 6: Image of the F1TENTH car used for evaluation equipped with the Intel NUC 10 computer (i7-10710U processor) and the Hokuyo UST-10LX LiDAR system.

Figure 7: Image of C-track with an overlay of the car state observation $\mathbf{O}_{car} = [v_x; v_y; \dot{\varphi}; d; \text{base}; v_{base}; \text{RL,prev}; v_{RL,prev}]^T$, denoted as shortened state vector in purple. The observation of the track information $\mathbf{O}_{track} = [p_{ref}^{0:J}; p_{left}^{0:J}; p_{right}^{0:J}]^T$ is depicted in yellow. The virtual boundaries (green: inside, purple: outside), and LiDAR scans are further included. Track-boundary violations during evaluation are automatically detected based on the virtual boundaries. The cones are placed as reference points for the human viewers.

(a) Turbo Tire

(b) TPU Tire

Figure 8: Images of the two tire types used during the experiments.

C Controller Comparison

Controller	t_{\min} [s]	t_{\max} [s]	t [s]	σ [s]	n_{bound}	T [min]
MAP Baseline	10.41	10.71	10.50	0.060	0	—
RL MAP	9.26	10.07	9.56	0.180	0	20.4
PP Baseline	12.06	12.18	12.13	0.033	0	—
RL PP	9.81	11.21	10.46	0.385	4	28.2
FTG Baseline	13.58	14.96	14.37	0.584	1	—
RL FTG	10.88	12.03	11.46	0.321	7	34.8
E2E RL	12.04	13.16	12.33	0.261	0	28.8
E2E RL	9.65	10.36	9.97	0.183	4	81.7

Table 2: Performance comparison of different baseline residual-controller combinations as well as the E2E controller on the C-track with Turbo tires after one battery life of training during 20 boundary-violation-free laps. t_{\min} represents the minimum lap time, t_{\max} the maximum lap time, t the average lap time, the standard deviation of the lap times, n_{bound} the number of boundary violations until 20 violation-free laps are reached, and T the total training time.

Figure 9: Lap Time vs. Wall Time during training for different residual controllers and the E2E controller, with respective reference for best lap time of the baseline controller when available. Only lap times without boundary violations are recorded. Lines start after the first collision-free lap. Only training for one battery life is shown.

D End-to-end Extended Results

Figure 10: Visualizations of the trajectory and speed profile of the [E2E](#) agent after 29 min of training on the C-track with Turbo tires during deployment.

Figure 11: Visualizations of the trajectory and speed profile of the E2E agent after 82 min of training on the C-track with Turbo tires during deployment.

Figure 12: Histogram of lap times of the E2E controller at 20 min and 82 min. Orange lines represent the MAP baseline (Min. Lap Time: dashed, Avg. Lap Time: solid).

E RL MAP Evaluation - Extended Results

Run	t_{\min} [s]	t_{\max} [s]	t [s]	[s]	n_{bound}	T [min]
C-Track, Turbo tires						
MAP Baseline	10.41	10.71	10.50	0.060	0	—
Seed 1	9.46	10.07	9.67	0.184	0	22.1
Seed 2	9.26	9.89	9.54	0.183	0	20.4
Seed 3	9.28	9.67	9.47	0.111	2	20.4
Combined Depl.	9.26	10.07	9.56	0.181	2	21.0
C-Track, TPU tires						
MAP Baseline	12.93	13.78	13.45	0.338	0	—
Seed 1	12.26	12.59	12.42	0.084	0	32.7
Seed 2	12.36	12.77	12.55	0.133	0	33.4
Seed 3	12.23	12.96	12.54	0.215	1	33.2
Combined Depl.	12.23	12.96	12.50	0.163	1	33.1
Y-Track, Turbo Tires						
MAP Baseline	8.55	8.68	8.62	0.045	0	—
Seed 1	7.57	7.96	7.76	0.126	1	24.8
Seed 2	7.87	8.26	8.05	0.126	0	21.7
Seed 3	7.87	8.46	8.11	0.151	5	21.2
Combined Depl.	7.57	8.46	7.97	0.205	6	22.6

Table 3: Performance of RL MAP across different tire-track combinations and weight initializations. t_{\min} represents the minimum lap time, t_{\max} the maximum lap time, t the average lap time, the standard deviation of the lap times, n_{bound} the number of boundary violations until 20 violation-free laps are reached, and T the total training time.

Figure 13: Stacked histogram of lap times across the different tire-track combinations and weight initializations, corresponding to Table 3. The orange lines represent the MAP baseline.

(a) C-Track, Turbo tires

(b) C-Track, TPU tires

(c) Y-Track, Turbo tires

Figure 14: Lap Time vs. Wall Time during training for [RL MAP](#) across different track-tire combination and seed initialization, corresponding to [table 3](#). The orange lines represent the [MAP](#) baseline.

Figure 15: Visualizations of the trajectory, speed profile and time delta of [RL MAP](#) (Seed 2) after 20 minutes of training on the track with TPU tires.

Figure 16: Visualizations of the trajectory, speed profile and time delta of [RL MAP](#) (Seed 1) after 20 minutes of training on the track with Turbo tires.

F Generalization

Extended results, reporting every seed's performance statistic on the generalization experiments are reported in Table 4.

Learning from scratch refers to the default training conducted in the rest of this work, and as such is a repetition of the results in Table 3, reported for ease of comparison. Zero-Shot Transfer refers to a policy trained on C-track and then deployed on Y-track without any additional training step, while Few-Shot Transfer refers to a policy trained on C-track and then deployed on Y-track after 20 minutes of additional training.

Run	t_{\min} [s]	t_{\max} [s]	t [s]	σ [s]	n_{bound}	T [min]
MAP Baseline	8.55	8.68	8.62	0.045	0	—
Learning from scratch						
Seed 1	7.57	7.96	7.76	0.126	1	24.8
Seed 2	7.87	8.26	8.05	0.126	0	21.6
Seed 3	7.87	8.46	8.11	0.151	5	21.2
Combined Depl.	7.57	8.46	7.97	0.205	6	22.6
Zero-Shot Transfer						
Seed 1	7.99	8.68	8.37	0.197	1	—
Seed 2	7.59	7.94	7.78	0.112	14	—
Seed 3	8.21	8.58	8.41	0.189	7	—
Combined Depl.	7.59	8.68	8.10	0.339	22	—
Few-Shot Transfer						
Seed 1	7.63	8.13	7.85	0.138	2	17.7
Seed 2	7.73	8.20	7.96	0.114	0	21.6
Seed 3	7.81	8.12	7.99	0.088	2	19.7
Combined Depl.	7.63	8.20	7.93	0.129	4	19.6

Table 4: Performance of RL MAP with few-shot and zero-shot transfer from C-track to the Y-track. t_{\min} represents the minimum lap time, t_{\max} the maximum lap time, t the average lap time, σ the standard deviation of the lap times, n_{bound} the number of boundary violations until 20 violation-free laps are reached, and T the total training time.

Figure 17: Visualizations of the trajectories during zero-shot transfer ~~C-track~~ to Y-track for Seeds 1, 2 and 3 (from top to bottom).

G Heuristic Delayed Reward Adjustment

Algorithm 1 Heuristic Delayed Reward Adjustment

Require: Replay buffer `replay_buffer`, current step index `current_step`

- 1: **Parameters:** adjustment_steps N , penalty p
- 2: **if** `terminal_state` **is** True **and** `replay_buffer.reward[current_step] = 0` **then**
- 3: **for** $n = 0$ to $N - 1$ **do**
- 4: `previous_step = current_step - n`
- 5: `current_reward = replay_buffer.reward[current_step]`
- 6: `decaying_penalty = p * n / (p + N)`
- 7: `adjusted_reward = current_reward - decaying_penalty`
- 8: `replay_buffer.reward[current_step - n] = adjusted_reward`
- 9: **end for**
- 10: **end if**

H Ablation Study Extended Results

Run	t_{\min} [s]	t_{\max} [s]	t [s]	[s]	n_{laps}	n_{bound}
HDRA+TD3, Sync	10.53	13.82	12.09	0.691	12.4	3.4
HDRA+TD3, Async	9.12	10.26	9.53	0.246	16.0	2.2
TD1, Async	9.73	20.81	11.53	2.823	11.0	5.6
TD3, Async	9.29	10.27	9.68	0.214	16.2	2.0

Table 5: Performance metrics summarized over five independent training runs, evaluating the last three minutes of 40 min-training runs during the ablation study on the simulated C-Track. The overall minimum, maximum, average lap time, and standard deviation are indicated with t_{\min} ; t_{\max} ; t ; respectively. The average over five runs of the number of laps and the number of boundary collisions in the three minutes is indicated with n_{laps} ; and n_{bound} ; respectively.

I Implementation Details

Category	Parameter	Value
Observations	Number of reference points J	20
	Look-ahead horizon l	6 m
Reward Design	Reward multiplier for progress	10
	Penalty p	10
	HDRA steps N	10
Safety Mechanisms	Safety filter δ_{filter}	$[-6; -2]$ rad
	Increment/decrement rate	0.05 rad
SAC Parameters	Optimizer	Adam
	Learning rate	0.003
	Discount factor	0.96
	Temporal-difference (TD) steps	3
	Replay buffer size	$1e^6$
	Batch size	256
	Number of hidden layers	2
	Size of hidden layers	256
Activations functions	ReLU	

Table 6: Hyperparameters for on-board RL.

J MPC Implementation Details

The MPC formulation used in this work uses a single-track bicycle model, with tire forces modeled with the *Pacejka Magic Formula* (Pacejka, 2012). The cost function is derived from the MPC formulation of Vázquez et al. (2020).

The model, expressed in curvilinear coordinates, reads as follows:

$$\dot{s} = ((v_x \cos \delta_{ref}) - (v_y \sin \delta_{ref})) = (1 - \kappa_{ref}(s) n) \dot{s} \quad (2)$$

$$\dot{n} = v_x \sin \delta_{ref} + v_y \cos \delta_{ref} \quad (3)$$

$$\dot{\delta}_{ref} = r - \kappa_{ref}(s) \dot{s} \quad (4)$$

$$\dot{v}_x = a + \frac{1}{m} (F_{yf} \sin \delta_{ref} + m v_y r) \quad (5)$$

$$\dot{v}_y = \frac{1}{m} (F_{yr} + F_{yf} \cos \delta_{ref} - m v_x r) \quad (6)$$

$$\dot{r} = \frac{1}{I_z} (F_{yf} l_f \cos \delta_{ref} - F_{yr} l_r) \quad (7)$$

where s represents the longitudinal advancement along the reference line, n the perpendicular lateral displacement, δ_{ref} the angle relative to the tangent at the point that meets the perpendicular, and $\kappa_{ref}(s)$ the curvature of the reference line at the corresponding s . The longitudinal input is modeled as a and the steering is δ_{ref} , resulting in the input $\mathbf{u} = (a; \delta_{ref})$. Longitudinal and lateral velocities are represented by $v_x; v_y$, respectively, and r represents the yaw rate. These latter three states are mostly influenced by tire forces, $F_{yf}; F_{yr}$, indicating the lateral tire force on the front and rear lumped tires, respectively. They follow the equations from the *Pacejka Magic Formula*:

$$F_{y,i} = F_{z,i} D_i \sin[C_i \arctan(B_i - E_i (B_i - \arctan(B_i - i)))] \quad (8)$$

where $i \in \{front; rear\}$ discriminates between front and rear tire. The slip angles δ_i are as follows:

$$\delta_f = \arctan\left(\frac{v_y + r\dot{\phi}}{v_x}\right) \quad (9)$$

$$\delta_r = \arctan\left(\frac{v_y - r\dot{\phi}}{v_x}\right) \quad (10)$$

The *Pacejka* parameters ($B_i; C_i; D_i; E_i$) are obtained via the procedure detailed by [Dikici et al. \(2025\)](#).

The *MPC* cost function, derived from [Vázquez et al. \(2020\)](#), is designed in order to follow the raceline (both on the positional and the velocity profile) computed by adjusting the minimum curvature raceline presented by [Heilmeier et al. \(2020\)](#) to the FITENTH vehicle. The *MPC* problem then approximately reads as follows:

$$\min_U l_f(\mathbf{x}_N) + \sum_{i=0}^{N-1} l(\mathbf{x}_i; \mathbf{u}_i) \quad (11)$$

$$\mathbf{x}_{i+1} = f(\mathbf{x}_i; \mathbf{u}_i) \quad \forall i \in \{0; \dots; N-1\} \quad (12)$$

$$\mathbf{x}_i \in \mathcal{X} \quad (13)$$

$$\mathbf{u}_i \in \mathcal{U} \quad (14)$$

$$\mathbf{x}_N \in \mathcal{X}_f \quad (15)$$

$$\mathbf{x}_0 = \hat{\mathbf{x}} \quad (16)$$

where:

- The state is $\mathbf{x} = [s; n; v_{ref}; v_x; v_y; r]^T$
- The number of timesteps is represented by N
- The state transition equation, derived from a *Runge-Kutta* discretization of the equations above, is displayed as $f(\mathbf{x}; \mathbf{u})$
- \mathcal{X} represents the track boundaries and state constraints sets
- \mathcal{U} represents the input constraints set
- $\hat{\mathbf{x}}$ is the measured state
- the cost function is $l(\mathbf{x}_i; \mathbf{u}_i) = W_n n + W_{v_{ref}} |v_{ref} - v_x| + W_{v_x} (v_x - v_x^{race})^2$, with v_x^{race} being the velocity obtained from the raceline generation
- $l_f(\mathbf{x}_i; \mathbf{u}_i) = 10l(\mathbf{x}_i; \mathbf{u}_i)$

Soft constraints are further integrated on state constraints, to try to ensure feasibility. The controller then is manually tuned for lap time minimization. The implementation is then carried out within the *acados* framework ([Verschueren et al., 2021](#)).

The *MPC* controller, in the end, did not achieve the fastest performance on the tires with the highest grip, and only achieved the fastest average lap time on the tires with the lowest grip. We attribute this performance gap to potential *sim-to-real* mismatches, such as unmodelled delays, as well as the higher signal noise inherent to the vehicle's sensor setup and embedded system constraints, which may have compromised the *MPC*'s performance and induced unnecessary conservativity.